

# Monolithically Integrated O-Band Coherent ROSA Featuring 2D Grating Couplers for Self-Homodyne Intra Data Center Links

Pascal M. Seiler<sup>ID</sup>, *Graduate Student Member, IEEE*, Galina Georgieva<sup>ID</sup>, Anna Peczek, Matthieu Oberon<sup>ID</sup>, Christian Mai<sup>ID</sup>, Stefan Lischke, Andrea Malignaggi<sup>ID</sup>, and Lars Zimmermann, *Senior Member, IEEE*

**Abstract**—In this work, we present an O-band dual-polarization coherent receiver optical sub-assembly (cROSA), monolithically integrated in a  $0.25\text{ }\mu\text{m}$  BiCMOS technology. The receiver features 248 nm deep ultra violet compatible 2-dimensional grating couplers (2D-GRCs), and an adaptive polarization controller, suitable for mitigation of local oscillator induced power fading in self-homodyne transmission systems. The cROSA is evaluated in system experiments at 64 GBd quadrature-phase shift-keying. Experimental results are related to grating coupler induced polarization crosstalk through Monte-Carlo simulations. Second generation 2D-GRCs are proposed.

**Index Terms**—BiCMOS, coherent communication, data center, ePIC, O-band, self-homodyne.

## I. INTRODUCTION

THE highly anticipated intra data center entry of coherent communication has shaped many of the industry's discussions in the past years. Critical for its implementation are the higher associated cost and power consumption of coherent communication compared to conventional direct-detect systems, rooted in the need for cooled narrow-linewidth tunable lasers and substantial digital signal processing (DSP). A number of key enablers have been identified, paving the way towards low cost and -power coherent intra data center links: 1) 2-dimensional grating couplers (2D-GRCs), featuring intrinsic polarization splitting and rotation [1], [2], and enabling low cost fabrication, testing, and assembly [3], [4]. 2) O-band coherent communication [5], [6], [7], [8], [9], [10], due to its reduced DSP complexity through

Manuscript received 24 March 2023; revised 18 April 2023; accepted 28 April 2023. Date of publication 2 May 2023; date of current version 10 May 2023. This work was supported by the German Research Foundation and the Open Access Publication Fund of TU Berlin. (*Corresponding author: Pascal M. Seiler.*)

Pascal M. Seiler and Lars Zimmermann are with the Department of Siliziumphotonik, Technische Universität Berlin, 10587 Berlin, Germany, and also with the IHP - Leibniz-Institut für Innovative Mikroelektronik, 15236 Frankfurt (Oder), Germany (e-mail: seiler@tu-berlin.de; lzimmermann@ihp-microelectronics.com).

Galina Georgieva and Matthieu Oberon are with the Department of Siliziumphotonik, Technische Universität Berlin, 10587 Berlin, Germany (e-mail: georgieva@tu-berlin.de; m.oberon@campus.tu-berlin.de).

Anna Peczek, Christian Mai, Stefan Lischke, and Andrea Malignaggi are with the IHP - Leibniz-Institut für Innovative Mikroelektronik, 15236 Frankfurt (Oder), Germany (e-mail: anna.peczek@ihp-microelectronics.com; cmai@ihp-microelectronics.com; lischke@ihp-microelectronics.com; malignaggi@ihp-microelectronics.com).

Digital Object Identifier 10.1109/JPHOT.2023.3272476

a severely limited chromatic dispersion. 3) Self-homodyne techniques, relying on a co-transmitted continuous wave tone to act as local oscillator (LO) at the receiver, can further simplify the DSP dedicated to carrier frequency offset and carrier phase recovery [11], [12], [13], [14]. Additionally, they enable un-cooled operation, as requirements regarding laser stability are heavily relaxed [12].

In this work, we present a fully integrated dual-polarization (DP) O-band coherent receiver optical sub-assembly (cROSA), featuring 2D-GRCs and an integrated polarization controller to mitigate LO-induced power fading. The monolithic cROSA has been fabricated in IHP's  $0.25\text{ }\mu\text{m}$  photonic BiCMOS technology [15]. The performance of the cROSA is evaluated in a system experiment at 64 GBd quadrature-phase shift-keying (QPSK). Compared to previous works [16], [17], we focus here on the evaluation of the 2D-GRC induced polarization crosstalk in real sub-systems. From the experimental results, the polarization crosstalk of the cROSA is estimated. This is done by the implementation of dedicated end-to-end Monte-Carlo simulations, which are adapted in this work to account for polarization crosstalk. Thus, limitations for higher-order modulation formats are determined. Finally, optimized 2D-GRCs are analyzed with regards to potential broadband polarization crosstalk suppression.

## II. PHOTONIC BiCMOS O-BAND CROSA

A photograph of the fabricated O-band cROSA is given in Fig. 1. Its total footprint is approximately  $11.5\text{ mm}^2$ . As optical interfaces, we have implemented 2D-GRCs for signal and LO, enabling intrinsic polarization splitting and rotation while supporting mature on-wafer testing using standard single-mode fibers. Note that the two orthogonal polarizations within the fiber are both converted to fundamental transversal electric (TE) modes by the 2D-GRCs, whereby one is denoted  $\text{TE}_X$  and the second  $\text{TE}_Y$  in this work (comp. Fig. 1). Polarization crosstalk in 2D-GRCs results due to the non-orthogonal splitting or combining of two polarization-multiplexed signals. In essence, this effect is equivalent to the polarization dependent loss (PDL)-induced crosstalk in the fiber transmission link [18]. Although this kind of crosstalk may be compensated in coherent detection systems by dedicated DSP, some penalties will be introduced [16], [19]. For that reason, the optimization of

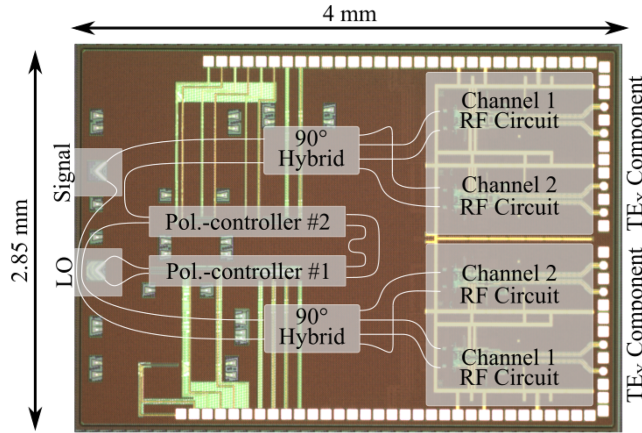


Fig. 1. Photograph of the fabricated cROSA, featuring 248 nm deep ultra violet compatible 2D-GRCs, an adaptive polarization controller, and a monolithically co-integrated electrical section. A detailed schematic of the polarization controller is given in Fig. 2(a).

individual components within our cROSA is of highest priority, with a more detailed analysis of the 2D-GRCs given in Section IV. The LO path also features an endless adaptive polarization controller, capable of adjusting the LO's random state of polarization incident at the cROSA's input, avoiding polarization-induced power fading. Note that in this scenario, the two orthogonally transmitted signals are still being demultiplexed in the DSP unit. In principle, a second adaptive polarization controller may be added to the signal path. However, the added insertion loss and complexity associated with an alignment routine, e.g. through training symbols, is unfavorable compared to a digital implementation. Alternative means to handle power fading in self-homodyne systems have been proposed in form of complementary coherent detection [14], though at the expense of additional signal processing. The controller implemented in this work is based on the combination of phase shifters and a Mach-Zehnder interferometer based on  $2 \times 2$  multi-mode interference couplers (MMIs), with a schematic given in Fig. 2(a). Note that, while the integrated controller is conceptually similar to the device presented in Ref. [12], a second polarization controller has been added in series for redundancy, as it allows to endlessly tune the device. While thermal tuning elements are most commonly used for these polarization controllers [12], [20], [21], we have used 250  $\mu\text{m}$  long p-i-n diodes for the cROSA in this work. The reasoning behind this is three-fold:

- 1) The use of p-i-n diodes allows for MHz tuning speeds, while thermal phase shifters are typically limited to below 10 kHz bandwidths. A normalized optical-electrical (OE) response of an exemplary diode is given in Fig. 2(b), showing a 3 dB bandwidth of approximately 26 MHz.
- 2) p-i-n diodes are highly efficient phase shifters at low modulation frequencies, thus enabling substantially lower power consumption compared to thermal tuning elements.
- 3) Crosstalk between thermal phase shifters can become a limiting factor, especially in a densely integrated implementation.

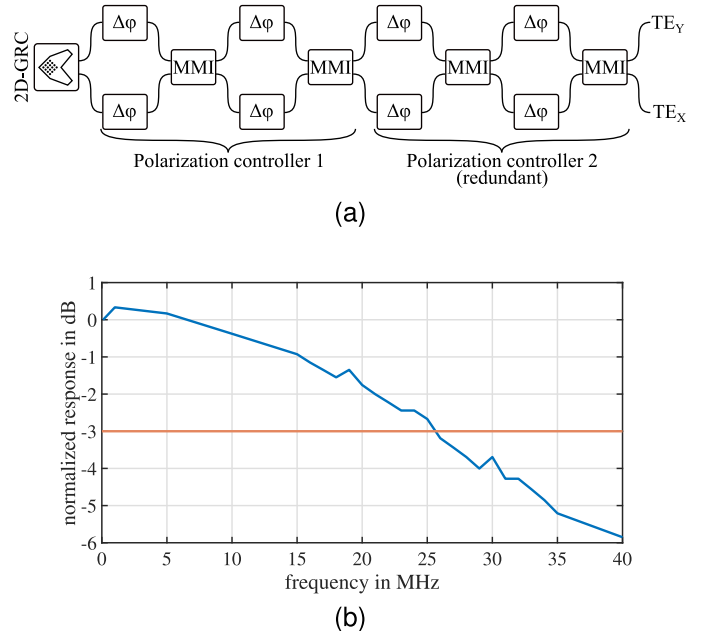


Fig. 2. (a) Schematic of the endless adaptive polarization controller, based on p-i-n diodes (indicated by  $\Delta\phi$ ) and multi-mode interference couplers (MMIs). (b) Normalized response of a p-i-n diode as used in the integrated polarization controller.

Drawback is a tuning-dependent attenuation, which has been characterized by applying a voltage to one of the phase shifters within the first polarization controller. Transmission characteristics measured at the  $\text{TE}_X$  and  $\text{TE}_Y$  outputs (comp. Fig. 2(a)), together with the combined signal  $\text{TE}_X + \text{TE}_Y$ , are given in Fig. 3(a). Note that the combined outputs are equivalent to the insertion loss induced by a single p-i-n diode. A  $V_\pi$  ( $2V_\pi$ ) tuning is typically associated with a  $<1$  dB ( $<2$  dB) increase in attenuation. Based on a measured I-V characteristic of an exemplary p-i-n diode given in Fig. 3(b), the power consumption at a  $2V_\pi$  tuning is approximately 10 mW.

The radio frequency (RF) circuit, schematically shown in Fig. 4(a) and based on the designs in Ref. [10], features an input differential transimpedance stage, variable gain amplifiers, output buffers, and two different loops, one performing automatic gain control and one devoted to direct current (DC) offset cancellation. Typically obtained OE 3 dB bandwidths based on this design are  $\geq 30$  GHz [10].

#### A. Experimental Setup

To validate the performance of the cROSA, we deploy the setup depicted in Fig. 4(b). We explicitly carry out an intradyne experiment rather than a self-homodyne, due to limited optical power and the lasers' operating wavelength during the measurement (1333 nm) being outside the bandwidth of the available fiber amplifiers. An O-band external-cavity laser (ECL) is fed to a DP C-band IQ modulator (DP IQ-MOD, ID photonics OMFT), where the 64 GBd electrical signals for the modulator's X- and Y-polarizations are supplied by an arbitrary waveform generator (AWG, Keysight M8199 A). Note that the experiment is limited to QPSK, due to the use of a commercial C-band modulator for

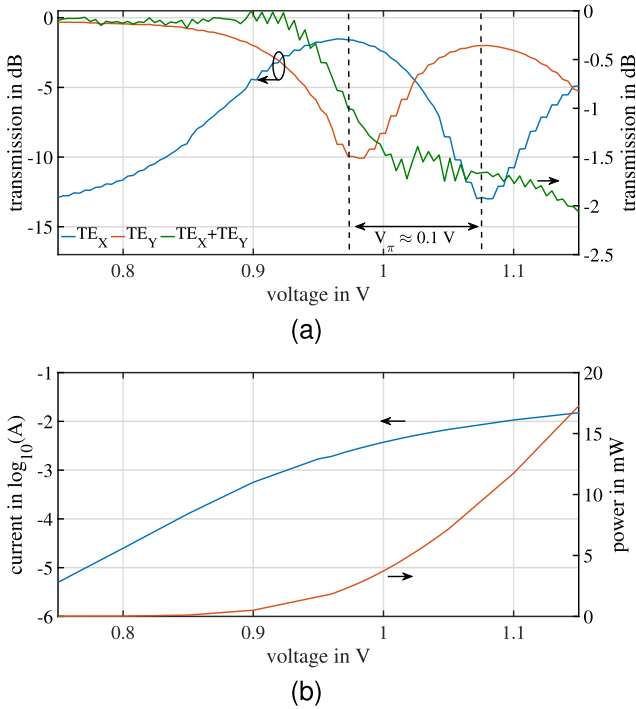


Fig. 3. (a) Output characteristic of the endless adaptive polarization controller when applying a voltage to one of the phase shifters. The Figure shows the individual outputs ( $\text{TE}_X$  and  $\text{TE}_Y$ ), as well as the combined output ( $\text{TE}_X + \text{TE}_Y$ ). (b) Measured current-voltage characteristic over applied voltage and respective power consumption for an exemplary p-i-n diode.

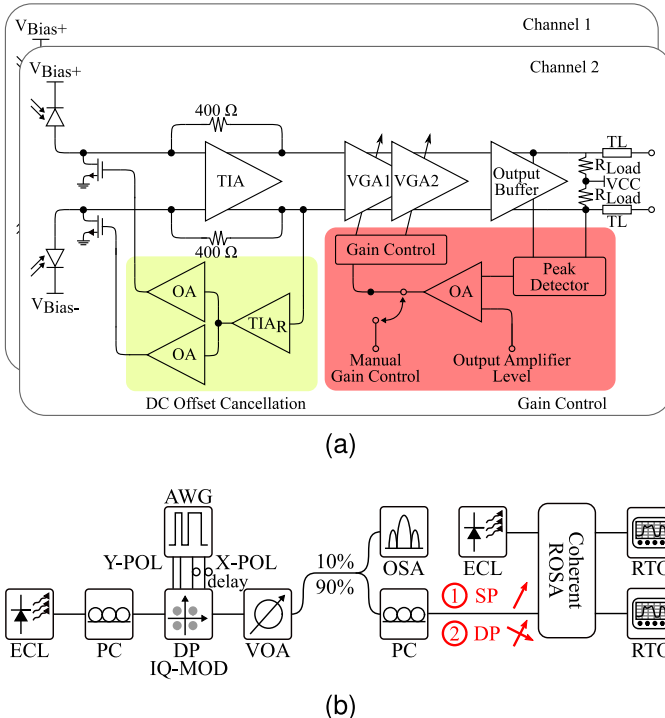


Fig. 4. (a) Monolithically integrated electrical output section (per polarization). ©2022 IEEE. Reprinted, with permission, from [10]. OA: operational amplifier, TIA: transimpedance amplifier,  $\text{TIA}_R$ : Replica TIA, VGA: variable gain amplifier, TL: transmission line,  $V_{Bias}$ : photodiode bias voltage. (b) Intradyne measurement setup. The red lettering indicates the two measurement scenarios. 1: single polarization incident at the cROSA. 2: dual polarization. PC: polarization controller, OSA: optical spectrum analyzer.

the O-band experiment. Since this cROSA is intended for intra data center applications and thus short reaches below 10 km, we use a variable optical attenuator (VOA) to adjust the received optical power (ROP) incident at the 2D-GRC. The cROSA is probed on-wafer using a fiber array and DC- and RF probes, and its electrical outputs are connected to two real-time oscilloscopes (RTO, Tektronix DPO77002SX) and analyzed offline using a commercial DSP-tool (Tektronix OM1106). The DSP prior to bit error counting entails clock recovery, phase estimation, matched filtering and least-mean-square equalization based on the symbol decision and a constant modulus algorithm (CMA). The LO (+12.3 dBm) is directly connected to the cROSA and polarization aligned on-chip using the integrated controller.

## B. Results

In commercial coherent transceivers, the two orthogonally transmitted signals are de-multiplexed in the DSP unit, but polarization crosstalk has to be kept small as to minimize associated penalties [16], [19]. To verify sufficiently low polarization crosstalk of the cROSA, we employ the following routine, indicated in Fig. 4(b) in form of the red enumeration. Due to the cROSA's size and the available RF probes, we only measure the  $\text{TE}_X$  polarization depicted in Fig. 1(a). First, a single-polarization (SP) signal is generated by turning off the electrical RF signal connected to the X-polarization at the IQ modulator. The signal is then manually polarization aligned to the 2D-GRC's output connected to the TE component in Fig. 1(a). This scenario is indicated by number 1 in Fig. 4(b). Bit error rates (BERs) are then measured at varied ROPs. Following, the DP signal is generated, as indicated by number 2 in Fig. 4(b). The polarization alignment for the DP signal remains unchanged to the SP scenario. Thus, we are measuring the penalty associated with the cROSA due to the polarization crosstalk induced by the 2D-GRC. Results for the BER over varied ROPs in the SP- and DP scenario are given in Fig. 5(a), where a linear fit has been added. Eye diagrams and constellations for the SP and DP scenario are shown in Fig. 5(b), (c) and (d), (e), respectively. The variations within a data set in Fig. 5(a) are related to drift in the manual fiber alignment during the measurement. Note that the ROP for the DP signal has to be intrinsically 3 dB higher compared to a SP signal. Removing that offset reveals a penalty  $\leq 0.5$  dB for all investigated ROPs.

## III. SIMULATION

Monte-Carlo simulations have been carried out in order to relate the experimentally determined penalty to a polarization crosstalk. The simulation system is based on the one used to obtain the results in Ref. [17], which has been extended in this work to include polarization crosstalk effects. All calculations are performed in MATLAB (MathWorks), and a schematic of the simulation setup is given in Fig. 6(a), with a list of essential simulation parameters given in Table I.

Note that the simulation parameters are chosen to relate to the experimental conditions, including specifications supplied by manufacturers, and typical characteristics of IHP's photonic

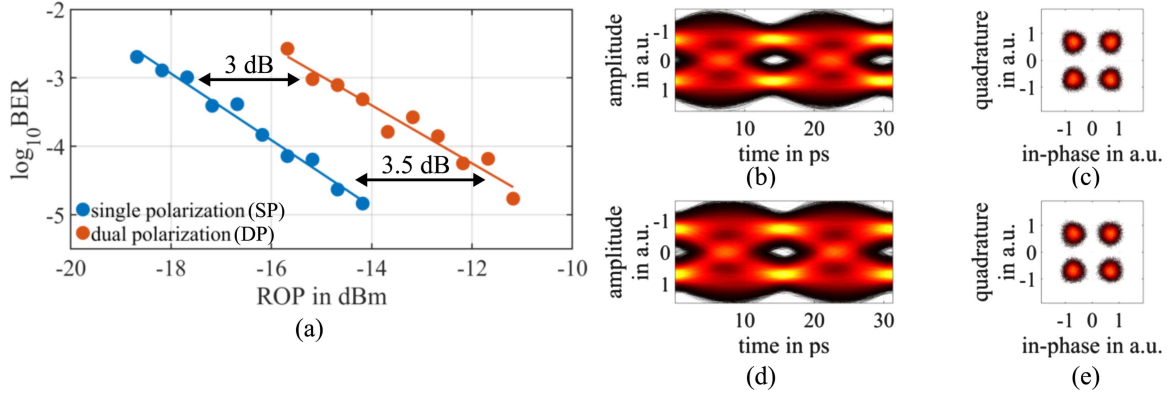


Fig. 5. (a) BERs for varied ROPs in the SP- and DP scenario at 64 GBd QPSK. Recovered eye diagrams and constellations for the (b, c) SP- ( $\text{ROP} = -14.2 \text{ dBm}$ ), and (d, e) DP scenario ( $\text{ROP} = -11.2 \text{ dBm}$ ). The eye diagrams have been resampled. The data are color-coded to an absolute bin count.

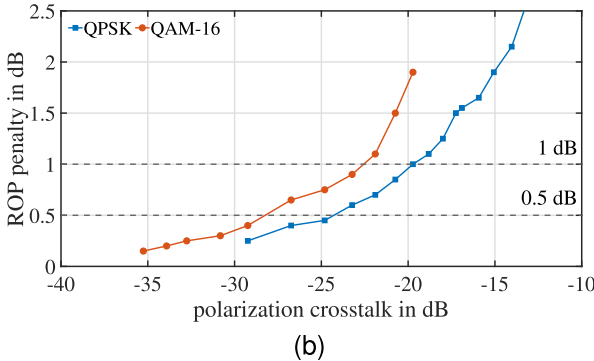
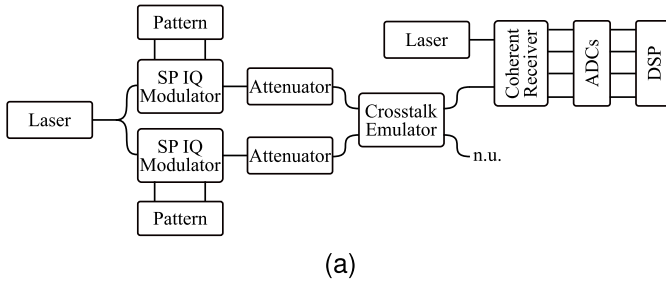


Fig. 6. (a) End-to-end link modeling simulation setup. n.u.: not used; ADC: analog-to-digital converter (b) Simulated ROP penalty relative to the case of no polarization crosstalk for varied crosstalks at a BER of  $1 \cdot 10^{-5}$  assuming QPSK and QAM-16.

TABLE I  
SIMULATION PARAMETERS

Parameter	Value
Wavelength	1333 nm
LO power	12.3 dBm
Laser relative intensity noise	-145 dB/Hz
Format	QPSK, QAM-16
Symbol rate	64 GBd
Pulse-shaping	root-raised-cosine
Roll-off factor	0.4
IQ modulator 3 dB bandwidth	36 GHz
Modulation depth	$1 V_\pi$
Photodiode 3 dB bandwidth	60 GHz
Photodiode dark current	100 nA
RF circuit 3 dB bandwidth	30 GHz
Input-referred noise current density	24 pA/ $\sqrt{\text{Hz}}$

BiCMOS technology. Results obtained through co-simulations of photonic sub-components, i.e. the  $90^\circ$  hybrid's wavelength dependent imbalance and phase error, are included [6]. The  $90^\circ$  hybrid is realized by a  $4 \times 4$  MMI based on a design routine similar to the one used to obtain the results in Ref. [22].

On the transmit side, the simulations consider the lasers' relative intensity noise, root-raised-cosine pulse-shaping, and bandwidth limitations, modeled as third-order Bessel-filters. Ideal Mach-Zehnder modulator transmission characteristics are assumed for the purpose of biasing and modulation. Two independent single polarization signals are generated, and subsequently interfered in a polarization crosstalk emulator. The procedure to model this effect is derived from previous analyses on crosstalk in polarization diverse systems [18]. To define polarization crosstalk, we assign the azimuth angle on the Poincaré sphere as  $2\psi$  and the zenith angle as  $2\chi$ . Two polarization states on the Poincaré sphere are characterized by the angles  $(2\psi_1, 2\chi_1)$  and  $(2\psi_2, 2\chi_2)$ . The polarizations are orthogonal to each other, when:

$$|\psi_2 - \psi_1| = \Delta\psi = 90^\circ$$

$$\chi_1 = -\chi_2.$$

Here, we consider  $\chi_1 = \chi_2 = 0$  and express the polarization crosstalk as:

$$m = \sin^2 \Delta\tilde{\psi} \quad (1)$$

where  $\Delta\tilde{\psi} = 90^\circ - \Delta\psi$  is a deviation from the orthogonal state. The derivation of the parameter  $m$  can be found in Ref. [16]. The cROSA is modeled after previously published devices [5], [6], and considers  $90^\circ$  hybrid non-idealities, shot noise, as well as an input-referred noise current induced by the co-integrated RF circuit. The DSP includes matched filtering, normalization, resampling, equalization based on a CMA [23], symbol demapping and bit error counting. Ideal carrier phase recovery is assumed, and frequency offsets between signal source and LO are omitted.

In order to relate the measured penalty to a polarization crosstalk, the simulation is first performed without crosstalk, and the attenuator in Fig. 6(a) is swept until a BER of  $1 \cdot 10^{-5}$

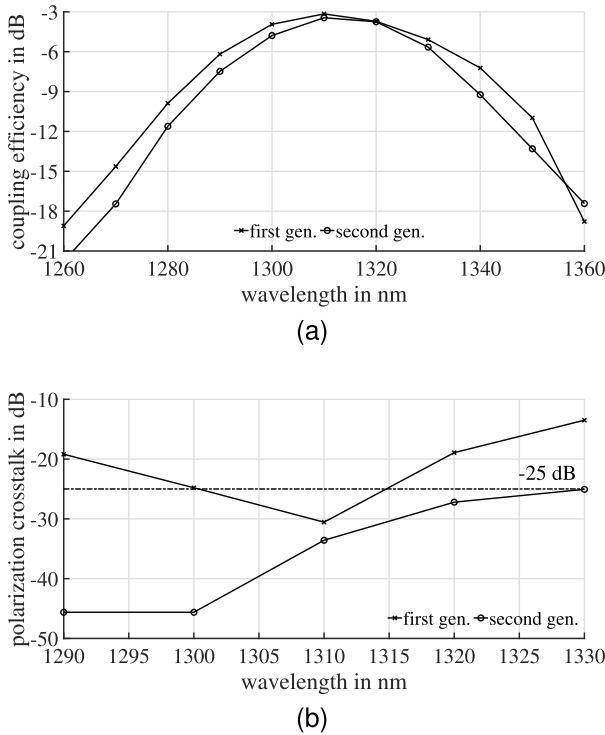


Fig. 7. Simulated comparison of the first- and second generation 2D-GRCs in terms of (a) coupling efficiency and (b) polarization crosstalk.

is achieved. The polarization crosstalk is then increased, and the penalty to the ROP for a BER of  $1 \cdot 10^{-5}$  is determined by decreasing the attenuation, with the results of that investigation shown in Fig. 6(b). Based on these simulations, the experimentally determined penalty of 0.5 dB at a BER of  $1 \cdot 10^{-5}$  for QPSK relates to a polarization crosstalk induced by the cROSA of approximately  $-25$  dB. Analogous simulations have been carried out for QAM-16, whereby the CMA has been exchanged for a radius directed least-mean-squares algorithm. As indicated in Fig. 6(b), the 2D-GRCs implemented in the cROSA support a ROP penalty for QAM-16 below 1 dB.

#### IV. FUTURE OPTIMIZATION

Albeit these first generation 2D-GRCs already enable excellent performance with ROP penalties below 1 dB for QPSK and QAM-16, further device optimization is desirable for future self-homodyne coherent detection systems, as the un-cooled laser operation implies a certain wavelength shift of the transmitted signal and LO. In order to be fully compliant with typical channel bandwidths of intra data center interconnects [24], we require a reliable performance in at least 20 nm bandwidth for our 2D-GRCs. The grating couplers used in our first generation cROSAs comprise circular perturbing elements. For this kind of 2D-GRC, it is known that low polarization crosstalk occurs in a limited wavelength range [16]. This is sufficient to achieve excellent results at a fixed wavelength, as demonstrated in the previous sections. To account for the demands of an un-cooled laser operation and higher-order modulation formats, a second generation 2D-GRC design is developed, using the zig-zag-tilt

technique from Refs. [2], [17] using elongated perturbing elements. Whereas the work presented in Ref. [17] focused on analysing the polarization dependency and coupling efficiency of the 2D-GRCs, this work aims to investigate the polarization crosstalk suppression. Fig. 7 compares the first- and second generation 2D-GRCs in terms of (a) coupling efficiency (TE<sub>x</sub> polarization as assigned in section II) as well as (b) polarization crosstalk. While both designs have similar coupling efficiency ( $-3.2$  dB vs.  $-3.4$  dB, without back-side reflector) and 1-dB-bandwidth (24 nm vs. 21 nm), the second-generation design maintains a crosstalk below  $-25$  dB over 40 nm bandwidth. This indicates also a good robustness against potential fabrication deviations.

#### V. CONCLUSION

To the best of our knowledge, we successfully demonstrated the first fully monolithic O-band cROSA suitable for self-homodyne intra data center interconnects. By use of a 248 nm deep ultraviolet lithography compatible 2D-GRC, low polarization crosstalk could be achieved. The integrated polarization controller based on p-i-n diodes can operate at MHz speeds and avoid LO-induced power fading. Future work shall focus on the implementation of the second generation 2D-GRCs and co-integration of control circuitry to automatically track the LO's random polarization, which can be easily implemented due to the monolithic approach. The device presented in this work paves the way toward cROSAs compliant with intra data center requirements regarding power consumption and cost.

#### REFERENCES

- [1] C.-W. Peng et al., "DP-QPSK coherent detection using 2D grating coupled silicon based receiver," *IEEE Photon. J.*, vol. 13, no. 1, Feb. 2021, Art. no. 7900105.
- [2] G. Georgieva, P. M. Seiler, C. Mai, A. Peczek, K. Petermann, and L. Zimmermann, "A polarization-independent zig-zag-tilted ovals grating coupler in a 0.25  $\mu\text{m}$  photonic BiCMOS technology," in *Proc. Eur. Conf. Opt. Commun.*, Basel, Switzerland, 2022, pp. 1–4.
- [3] T. Pinguet et al., "High-volume manufacturing platform for silicon photonics," *Proc. IEEE*, vol. 106, no. 12, pp. 2281–2290, Dec. 2018.
- [4] R. Marchetti, C. Lacava, L. Carroll, K. Gradowski, and P. Minzioni, "Coupling strategies for silicon photonics integrated chips [Invited]," *Photon. Res.*, vol. 7, no. 2, Jan. 2019, Art. no. 201.
- [5] P. M. Seiler et al., "56 GBaud O-band transmission using a photonic BiCMOS coherent receiver," in *Proc. Eur. Conf. Opt. Commun.*, Brussels, Belgium, 2020, pp. 1–4.
- [6] P. M. Seiler et al., "Toward coherent O-band data center interconnects," *Front. Optoelectron.*, vol. 14, no. 4, pp. 414–425, Dec. 2021.
- [7] H. Andrade, Y. Xia, A. Maharry, L. Valenzuela, J. Buckwalter, and C. Schow, "50 GBaud QPSK 0.98 pJ/bit receiver in 45 nm CMOS and 90 nm silicon photonics," in *Proc. Eur. Conf. Opt. Commun.*, Bordeaux, France, 2021, pp. 1–4.
- [8] T. Hirokawa et al., "Analog coherent detection for energy efficient intra-data center links at 200 Gbps per wavelength," *J. Lightw. Technol.*, vol. 39, no. 2, pp. 520–531, Jan. 2021.
- [9] A. Maharry et al., "First demonstration of an O-band coherent link for intra-data center applications," in *Eur. Conf. Opt. Commun.*, Basel, Switzerland, 2022, pp. 1–4.
- [10] P. M. Seiler et al., "Multiband silicon photonic ePIC coherent receiver for 64 GBd QPSK," *J. Lightw. Technol.*, vol. 40, no. 10, pp. 3331–3337, May 2022.
- [11] M. Y. S. Sowailem et al., "Self-homodyne system for next generation intra-datacenter optical interconnects," *Opt. Exp.*, vol. 25, no. 22, Oct. 2017, Art. no. 27834.

- [12] T. Gui, X. Wang, M. Tang, Y. Yu, Y. Lu, and L. Li, "Real-time demonstration of 600 Gb/s DP-64QAM self-homodyne coherent Bi-direction transmission with un-cooled DFB laser," in *Proc. Opt. Fiber Commun. Conf. Exhib.*, San Diego, California United States, 2020, pp. 1–3.
- [13] Y. Gao, X. Zhou, F. Li, J. Huo, J. Yuan, and K. Long, "Mismatch length estimation of self-homodyne coherent optical systems by using carrier-pilot-assist method," in *Proc. Opt. Fiber Commun. Conf.*, 2022, pp. 01–03.
- [14] H. Ji et al., "Complementary polarization-diversity coherent receiver for self-coherent homodyne detection with rapid polarization tracking," *J. Lightw. Technol.*, vol. 40, no. 9, pp. 2773–2779, May 2022.
- [15] S. Lischke, D. Knoll, C. Mai, and L. Zimmermann, "Advanced photonic BiCMOS technology with high-performance Ge photo detectors," *Proc. SPIE*, vol. 11088, pp. 46–56, 2019.
- [16] G. Georgieva, M. Sena, P. M. Seiler, K. Petermann, J. Fischer, and L. Zimmermann, "Penalties from 2D grating coupler induced polarization crosstalk in silicon photonic coherent transceivers," *IEEE Photon. J.*, vol. 14, no. 5, Oct. 2022, Art. no. 6653011.
- [17] L. Zimmermann, P. M. Seiler, C. Mai, and G. Georgieva, "Toward 2D grating coupler enabled O-band coherent links based on SiGe photonic electronic technology," *Japanese J. Appl. Phys.*, vol. 62, no. SC, Feb. 2023, Art. no. SC0807.
- [18] H.-C. Ji, J. H. Lee, H. Kim, P. K. J. Park, and Y. C. Chung, "Effect of PDL-induced coherent crosstalk on polarization-division-multiplexed direct-detection systems," *Opt. Exp.*, vol. 17, no. 3, pp. 1169–1177, Feb. 2009.
- [19] C. Xie, "Impact of nonlinear and polarization effects in coherent systems," *Opt. Exp.*, vol. 19, no. 26, pp. B915–B930, Dec. 2011.
- [20] W. D. Sacher et al., "Polarization rotator-splitters and controllers in a Si<sub>3</sub>N<sub>4</sub>-on-SOI integrated photonics platform," *Opt. Exp.*, vol. 22, no. 9, May 2014, Art. no. 11167.
- [21] P. Velha et al., "Wide-band polarization controller for SI photonic integrated circuits," *Opt. Lett.*, vol. 41, no. 24, Dec. 2016, pp. 5656–5659.
- [22] L. Zimmermann, K. Voigt, G. Winzer, K. Petermann, and C. Weinert, "C-Band optical 90-Hybrids based on silicon-on-insulator 4 × 4 waveguide couplers," *IEEE Photon. Technol. Lett.*, vol. 21, no. 3, pp. 143–145, Feb. 2009.
- [23] J. Proakis, *Digital Communications*, 4th ed. Boston, MA, USA: McGraw-Hill, 2001.
- [24] 800 G Pluggable MSA, "800G-FR4 Technical Specification," 2021. Accessed: Dec. 5, 2022. [Online]. Available: [800gmsa.com/documents/800g-fr4-2km-specification-v10](http://800gmsa.com/documents/800g-fr4-2km-specification-v10)